Shannon Information of Synaptic Weights Post Induction of Long-Term Potentiation (Learning) is Nearly Maximized

Anonymous Author(s)
Affiliation
Address
email

Abstract

We have applied Shannon information theory to obtain a new analysis of synaptic information storage capacity (SISC) using non-overlapping dimensions of dendritic spine head volumes as a measure of synaptic weights with distinct states. Spine head volumes in the stratum radiatum of hippocampal area CA1 occupied 24 distinct states (4.1 bits). In contrast, spine head volumes in the middle molecular layer of control dentate gyrus occupied only 5 distinct states (2 bits). Thus, synapses in different hippocampal regions had different synaptic information storage capacities. Moreover, these were not fixed properties but increased during long-term potentiation, such that by 30 min following induction, spine head volumes in the middle molecular layer increased to occupy 10 distinct states (3 bits), and this increase lasted for at least 2 hours. Measurement of the Kullback-Liebler divergence revealed that synaptic states evolved closer to storing the maximum amount of information during long-term potentiation. SISC revealed that the Shannon information after long-term potentiation is nearly maximized for the number of distinguishable states.

1 Introduction

Synapses between neurons control the flow of information in neural circuits and their strengths are regulated by experience. Dendritic spine head volumes are known as a surrogate for synaptic strength/weight. While synaptic plasticity is well-established as an experience-dependent mechanism for modifying spine head volumes and other synaptic features, the precision of the mechanism is unknown. From an information theory point of view, there can be no information stored without precision – the more precise synaptic plasticity is, the more distinguishable synaptic strength states are possible and the greater amount of information that can be stored at the synapses in a particular neural circuit. Pairs of synapses from the same axon on the same dendritic branch (Called same-dendrite same-axon pairs (Bartol et al, 2015) or joint synapses on different dendritic branches (Motta et al., 2019; Dorkenwald et al, 2019) have highly correlated sizes due to common history of coactivation and consequently have similar spine head volumes, suggesting that changes in synapse structure are precisely modulated (Bartol et al, 2015; Kasthuri et al., 2015; Bloss et al., 2018).

Until recently the measurement techniques did not have the potential to measure the precision of synaptic plasticity because the measurement error from the actual sizes of synapses were much higher than potential synaptic plasticity mechanism error. Exploring same-dendrite same-axon synapse pairs for measuring precision of synaptic plasticity and information encoding in synapses is foundational to understanding mechanisms of learning and memory and studying aging and neurodegenerative

Submitted to Information-Theoretic Principles in Cognitive Systems Workshop at the 36th Conference on Neural Information Processing Systems (NeurIPS 2022). Do not distribute.

diseases such as Alzheimer's disease as well as improving artificial intelligence algorithms and building neuromorphic computers.

We analyzed high-resolution 3-dimensional electron microscopy (3DEM) reconstructed spine head volumes, a surrogate for synaptic strength, in hippocampal area CA1 and dentate gyrus in rat and measured the precision of synaptic plasticity, quantified information capacity per synapse, explored the effect of long-term potentiation (LTP) on the aforementioned metrics, and finally explored the efficiency of coding in synapses by analyzing spine head volumes in multiple conditions. We performed our analysis on 5 datasets (3 control datasets and 2 in vivo induced LTP on freely moving rats; see Appendix subsection (Induction of LTP in the Dentate Gyrus) and Supplemental Fig. 2 for detail information) coming from 3DEM reconstructed dendrites of hippocampal area CA1 and dentate gyrus (N=5 rats), while other recent works performed analysis on single mice in control condition (Motta et al., 2019). In our study, we noticed synapses in different hippocampal regions had different synaptic information storage capacities. Our results revealed that synaptic states evolved closer to storing the maximum amount of information during long-term potentiation and are nearly maximized for the number of distinguishable states.

2 Figures

"The fundamental problem of communication is that of reproducing at one point either exactly or approximately a message selected at another point. Frequently the messages have meaning; that is they refer to or are correlated according to some system with certain physical or conceptual entities. These semantic aspects of communication are irrelevant to the engineering problem. The significant aspect is that the actual message is one selected from a set of possible messages. The system must be designed to operate for each possible selection, not just the one which will actually be chosen since this is unknown at the time of design." (Shannon, 1948)

Shannon's information theory is the rigorous basis for a new method to quantify empirically SISC; that is, the number of bits of Shannon entropy stored per synapse. For this new method, only the precision as measured by the coefficient of variation (CV) of SDSA pairs, presented in Table 1, was borrowed from Bartol et al. (2015). The new method performs non-overlapping cluster analysis using Algorithm 2, to obtain the number of distinguishable categories of spine head volumes from the CV measured across the reconstructed dendrites (Fig. 1).

The Shannon information per synapse is calculated by using the frequency of spine head volumes in the distinguishable categories where each category is a different message for the calculation of Shannon information. The maximum number of bits is calculated as the log2(N_c) where N_c is the number of categories which set an upper bound for the SISC.

When calculating the amount of entropy per synapse, the random variable is the synapse size and the number of distinguishable synaptic states is the realization of a random variable for the occurrence of each state. The probability of the occurrences of each state is calculated by the fraction of the number of spine head volumes in each of the clusters over the total number of spine head volumes in the reconstructed volume. The information coding efficiency at synapses is measured by Kullback-Leibler (KL) divergence to quantify the difference between two probability distributions, one from the categories of spine head volumes and the other from a corresponding uniform distribution with the same number of categories. (A uniform distribution is the maximum entropy discrete probability distribution when there is no constraint on the distribution except having the sum of the probabilities equal 1.)

3 Discussion

This paper introduces a new analytical approach for determining SISC that has several advantages over our prior approach (Bartol et al., 2015). The new method was used on data from area CA1 to compare it with the prior approach. It was then applied to track SISC changes in the Dentate Gyrus at 30 minutes and 2 hours following the induction of LTP. The analyses revealed that synaptic precision, based on covariance of spine head volume in SDSA pairs, was not altered. This finding suggests that as one spine of the pair enlarged (or shrank) following LTP, the other spine head changed in tandem. The number of distinguishable synaptic strengths was increased by LTP by altering the range and frequency of spine head volumes. At 30 minutes, spine head size shifted from the middle of

the range both towards smaller and larger sizes. These shifts increased the number of bits from 2.0 in the control conditions for both time points to 3.0 bits after 30 min and 2.7 bits at 2 hr following induction of LTP. These outcomes were a consequence of increases in both larger and smaller spine head volumes, which broadened the size distributions, bringing them closer to the optimal uniform Shannon distribution. This broadening in size range was observed in both the 30 min and the 2 hr difference distributions. As a consequence, the information storage capacity was increased by around 50% following LTP, an increase that was preserved between 30 min and 2 hr. However, there was evidence for further reorganization of spine head volumes after 30 min since the KL divergence between the distribution of spine head volumes and the optimal uniform distribution at 2 hr was half that of the control, thereby using the range of spine head volume sizes more efficiently. Thus, the amount of information that a population of synapses can store is not fixed but can be expanded toward the Shannon limit.

Table 1: The number of distinguishable states, or categories, $(\mathrm{N_c})$ of spine head volumes.

Dataset Type	# SDSA pairs	Median CV	# SHV	Median SHV (μm^3)	SRF	N_c
DG 30 min Con	10	0.65 ± 0.12	209	0.031 ± 0.0037	73	5
DG 30 min LTP	8	0.37 ± 0.16	188	0.022 ± 0.0014	236	10
DG 2 hr Con	18	0.56 ± 0.09	239	0.023 ± 0.0013	110	6
DG 2 hr LTP	10	0.42 ± 0.15	226	0.031 ± 0.0036	141	8

Table 1: For column 3 and 5 the term ($\pm$ SEM), SEM stands for standard error of median calculated using algorithm 1.

Table 2: Calculating the entropy of synaptic weights based on the calculated frequency of distinguishable synaptic states.

Dataset	Shannon Entropy (P)	Maximum Entropy (Q)	$\mathrm{KL(P\|Q)}$	$\mathrm{KL/KL_{MAX}}$
30 min Control	2.0 ± 0.32	2.32 ± 0.34	0.33 ± 0.1	0.14 ± 0.045
30 min LTP	3.0 ± 0.42	3.32 ± 0.42	0.32 ± 0.089	0.096 ± 0.035
2 hr Control	2.05 ± 0.27	2.59 ± 0.29	0.53 ± 0.10	0.21 ± 0.040
2 hr LTP	2.74 ± 0.41	3.0 ± 0.41	0.26 ± 0.086	0.086 ± 0.038
CA1	4.1 ± 0.39	4.6 ± 0.37	0.49 ± 0.068	0.11 ± 0.021

Tâble 2: For coolumn 2-5 the term ($\pm$ SE), SE stands for standard eprop calculatéd with bootstrapping using algorithm 1 and 2, concurrently.

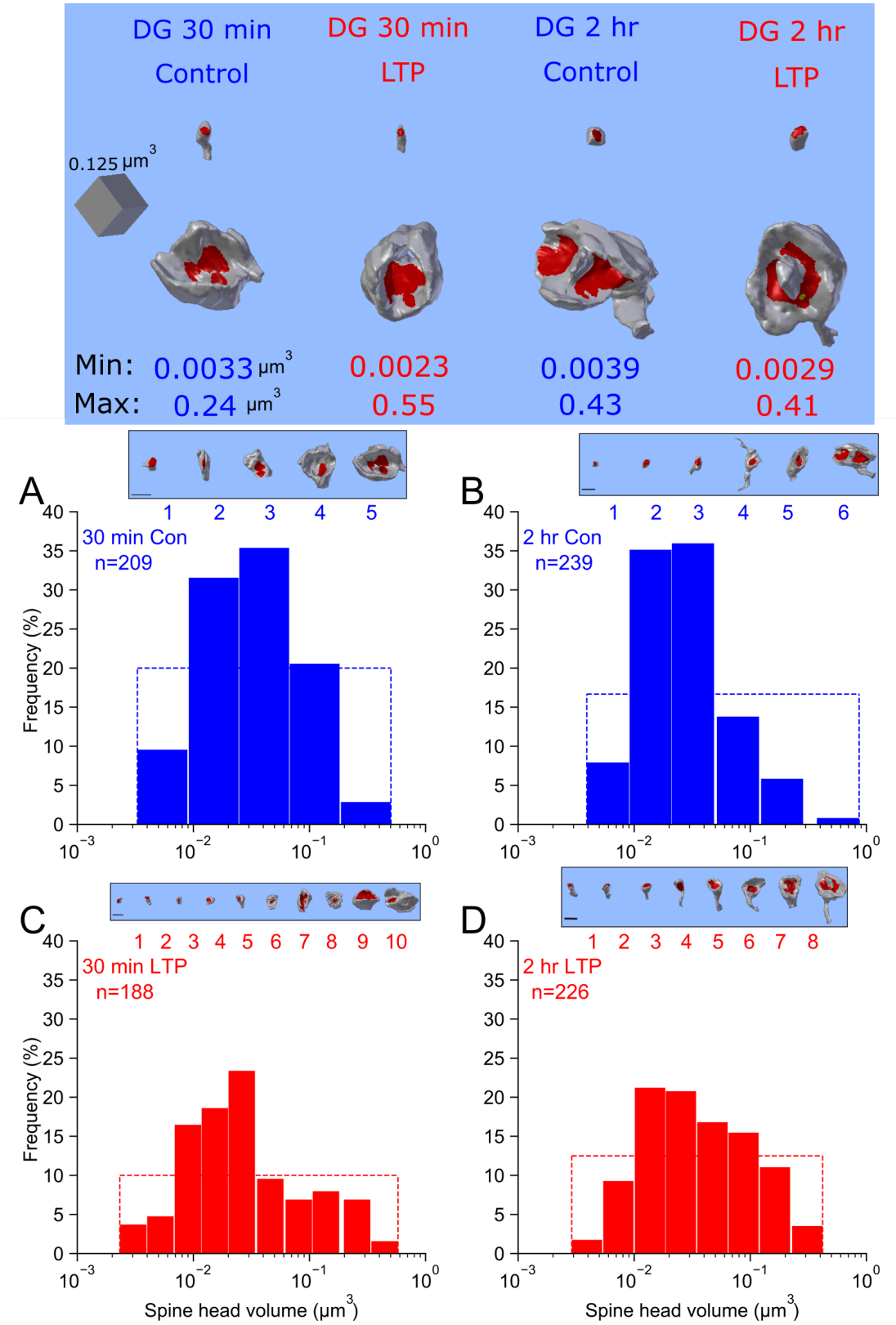

Figure 1: Clustering of spine head volumes in Dentate Gyrus datasets before and after LTP. Clustering algorithm 2 was used, to show that following LTP there was an increase in N_c. Here categories are illustrated as histogram bins with bin-width equal to the CV shown in Table 1.

Figure 1: Blue and red colors indicate Control and LTP conditions, respectively. For each panel the Y axis shows the counts of spine head volume in the respective bin divided by total number of spine head volumes in the given dataset. The X axis shows the spine head volumes in μm^3 log scale. (A) Dentate Gyrus 30 min Control, (B) Dentate Gyrus 2 hr LTP, (C) Dentate Gyrus 30 min LTP, (D) Dentate Gyrus 2 hr LTP. The rectangular inset on the top of each histogram shows the largest spine head and category number of each category and aligns with the X axis of the category histogram. For comparison of each histogram to the shape of a uniform distribution, the dashed line indicates the theoretical uniform distribution (and maximum entropy and Shannon information) for the given dataset.

References

[1] Bartol TM, Bromer C, Kinney J, Chirillo MA, Bourne JN, Harris KM, Sejnowski TJ. Nanoconnectomic upper bound on the variability of synaptic plasticity. Elife. 2015; 4:e10778.

[2] Motta A, Berning M, Boergens KM, Staffler B, Beining M, Loomba S, Hennig P, Wissler H, Helmstaedter M. Dense connectomic reconstruction in layer 4 of the somatosensory cortex. Science. 2019; 366(6469).

[3] Bloss, C.S., Wineinger, N.E., Peters, M., Boeldt, D.L., Ariniello, L., Kim, J.Y., Sheard, J., Komatireddy, R., Barrett, P. and Topol, E.J., 2016. A prospective randomized trial examining health care utilization in individuals using multiple smartphone-enabled biosensors. PeerJ, 4, p.e1554.

[4] Kasthuri, N., Hayworth, K.J., Berger, D.R., Schalek, R.L., Conchello, J.A., Knowles-Barley, S., Lee, D., Vázquez-Reina, A., Kaynig, V., Jones, T.R. and Roberts, M., 2015. Saturated reconstruction of a volume of neocortex. Cell, 162(3), pp.648-661.

[5] Smith, H.L., Bourne, J.N., Cao, G., Chirillo, M.A., Ostroff, L.E., Watson, D.J. and Harris, K.M., 2016. Mitochondrial support of persistent presynaptic vesicle mobilization with age-dependent synaptic growth after LTP. Elife, 5, p.e15275.

[6] Dobrunz, L.E. and Stevens, C.F., 1997. Heterogeneity of release probability, facilitation, and depletion at central synapses. Neuron, 18(6), pp.995-1008.

[7] Dorkenwald S, Turner NL, Macrina T, Lee K, Lu R, Wu J, Bodor AL, Bleckert AA, Brittain D, Kemnitz N, et al. Binary and analog variation of synapses between cortical pyramidal neurons. bioRxiv. 2019.

[8] A. Anonymous.

[9] Bowden JB, Abraham WC, Harris KM. Differential effects of strain, circadian cycle, and stimulation pattern on LTP and concurrent LTD in the dentate gyrus of freely moving rats. Hippocampus. 2012; 22(6):1363–1370.

[10] Bromer C, Bartol TM, Bowden JB, Hubbard DD, Hanka DC, Gonzalez PV, Kuwajima M, Mendenhall JM, Parker PH, Abraham WC, et al. Long-term potentiation expands information content of hippocampal dentate gyrus synapses. Proceedings of the National Academy of Sciences. 2018; 115(10):E2410–E2418.

Appendix

Major results of our study:

1. We used high-resolution 3DEM reconstructed volumes to measure the precision of synaptic plasticity in 5 rats in both control and LTP conditions.
2. We quantified Shannon Information at the synaptic level for the first time. Information Theory has been applied to the spike trains analysis (Dayan, and Abbott, 2005) but has not previously been used to measure synaptic strength.
3. We explored variations in synaptic information capacity 30 min and 2 hours after inducing on freely moving rats, which has not previously been studied.
4. Our methods and computational tools will be made available to the public as well as all the 3DEM datasets.

Standard error of median

Exploring different aspects of synaptic plasticity processes in the hippocampus is crucial to understanding mechanisms of learning and memory, improving artificial intelligence algorithms, and

neuromorphic computers. Synapses from the same axon onto the same dendrite have a common history of coactivation and have similar spine head volumes, suggesting that synapse function precisely modulates structure.

The standard error of median for the precision levels of each of the 5 dataset's SDSA pairs is calculated with Algorithm 1 as follows. The idea is to generate 1000 bootstrap samples of length n, each sampled from the n SDSA pairs with replacement, to estimate the standard error of median for the n SDSA pairs (Table 1, column 3). The standard error of median of spine head volumes follows the same procedure using Algorithm 1.

Algorithm 1 Bootstrap Algorithm for Estimating the Standard Error of Median

Require: $n \geq 1$

Let $X_1, \ldots, X_n$ be some data and $\hat{\theta}_n = t\left(X_1, \ldots, X_n\right)$

For $b = 1, \ldots, B$

Simulate $X_1^{*(b)}, \ldots, X_n^{*(b)} \overset{iid}{\sim} F_n$ by sampling with replacement from $\{X_1, \ldots, X_n\}$

Evaluate $\hat{\theta}_n^{*(b)} = t\left(X_1^{*(b)}, \ldots, X_n^{*(b)}\right)$

$$\hat{\sigma}_{n,B}^2 = \frac{1}{B}\sum_{b=1}^{B}\left(\hat{\theta}_n^{*(b)} - \frac{1}{B}\sum_{b=1}^{B}\hat{\theta}_n^{*(b)}\right)^2$$

Return the bootstrap estimate of standard error of median

$$\hat{\sigma}_{n,B}$$

Clustering

To construct the clusters, spine head volumes are sorted from smallest to the largest. The first value (smallest value) is selected and the CV of that value and the remaining head volumes are calculated in a pairwise manner. The head volumes for which the calculated CV is below the threshold (the median value of the SDSA pairs CV) are assigned to the first category and deleted from the pool of N spine head volumes. This procedure is repeated until the CV exceeds the median SDSA pairs CV and a new category is formed. New categories are formed until all the remaining spine head volumes are assigned to a category and the original vector of spine head volumes is empty (see Algorithm 2 for details). It is guaranteed that the coefficient of variation between each random pair within each category is less than the threshold value measured from the reconstructed tissue SDSA pairs. All spine head volumes are rounded to two significant digits for the display.

Algorithm 2 Clustering Algorithm

function PRECISION CALCULATION((Same Dendrite Same Axon pairs (SDSA), N pairs (a,b) of spine head volumes))
    for $a, b \in SDSA[i]$ **do**
$cv = \sigma/\mu$
CV[i]=cv
    end for
    return $\{Median(CV)\}$
end function
function CLUSTERING SPINE HEAD VOLUMES(SHV vector)
    Sort SHV s.t. $SHV[i] < SHV[i+1]$
    $Listofshcluster = NULL$
    while $Length(SHV) \neq 0$ **do** ▷ Here we do the clustering with the median value of SDSA pairs calculated with the above function.
        a= SHV[1]
        for any $b \in SHV$ **do**
            Cluster=NULL
            if $cv(a, b) < Median(CV)$ **then**
                $Cluster \leftarrow b$
            end if
        end for
        $Listofshcluster[j] \leftarrow Cluster$
        $SHV = SHV[-Cluster]$(deleting the spine head volumes stored in cluster j from the SHV vector)
        j=j+1
    end while
    return $\{Listofshcluster\}$ and $N_c = j - 1$
end function

.1 Induction of LTP in the Dentate Gyrus

We analyzed 3D reconstruction from serial section electron microscopy (3DEM) datasets containing perforant path synapses in the middle molecular layer (MML) of the Dentate Gyrus for inputs arising from the medial entorhinal cortex. Data were collected from the stimulated hippocampus of two rats at 30 min and two rats at 2 hours post-induction of LTP, with the hippocampus in the opposite hemisphere serving as the control. All experiments were conducted in the middle of the animals' waking (dark) period to control for variation due to the circadian cycle (Bowden et al., 2012). Analysis of the 30 min control and LTP datasets using our previous signal detection method (Bartol et al., 2015) was published in Bromer et al. (2018). We used the previously described methods to induce LTP in the MML of freely moving rats (Bowden et al., 2012). Briefly, stimulating electrodes were surgically implanted in both the medial and lateral perforant paths of the LTP hemisphere, and an additional stimulating electrode was implanted in the medial path of the control hemisphere. Field potential recordings were made using electrodes placed bilaterally in the dentate hilus. Animals were allowed to recover for two weeks prior to producing LTP or control stimulation during the animals' dark (waking) part of the circadian cycle. LTP was induced by 50 trains of unilateral delta-burst stimulation to the medial path electrode and then recorded for either 30 min or 2 hr, timed from the beginning of the delta-burst stimulation. Relative to the two control hemispheres, the LTP hemispheres showed an average of 41% potentiation in the MML for the 30 min experiment (Supplemental Fig. 2A, B). In the 2 hr experiment, there was an average of 37% LTP for the two animals (Supplemental Fig. 2C). Serial electron micrographs and 3D reconstructions were prepared from the control (Supplemental Fig. 2D) and 30 min LTP (Supplemental Fig. 2E) hemispheres of two animals, and the control (Supplemental Fig. 2F) and 2 hr LTP (Supplemental Fig. 2G) hemispheres of the other two animals. Three-dimensional reconstructions were made for all of the dendritic spines and synapses occurring along three dendritic segments from each of the control and LTP hemispheres for a total of 24 dendrites and 862 dendritic spines. Axons that were presynaptic to at least 1 of 15 dendritic spines located along the middle of the dendritic segment were traced to determine whether they made more than one synapse along the same dendrite, and thus formed SDSA pairs. All 3D reconstructions and measurements were obtained blind as to condition or animal.

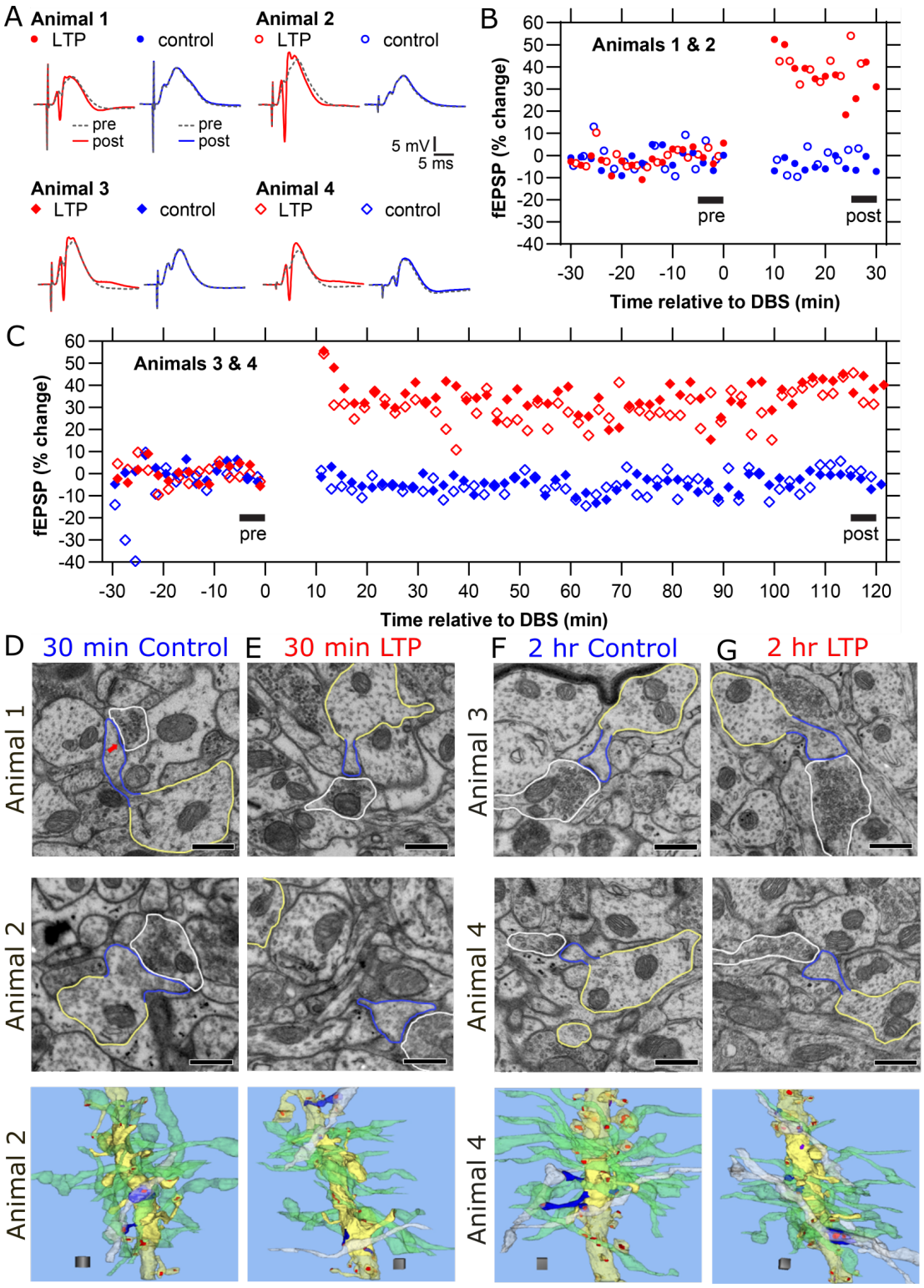

Figure 2: LTP and control responses monitored for 30 min and 2 hours prior to preparation for 3DEM, and representative dendrites from the control and LTP hemispheres in MML.

Figure 2: (A) Plots in panel A show representative waveforms from baseline responses (dotted, pre) superimposed on responses following delta-burst stimulation (solid, post) in the LTP (red) or control (blue) hemispheres. (Unique symbols are indicated for each animal and plotted in B and C). (B) Change in fEPSP slopes relative to baseline stimulation in the LTP (red) or control (blue) hemispheres monitored for 30 minutes prior to fixation. The average change relative to baseline stimulation in fEPSP response was 34% and 48% at 30 minutes post-LTP induction and 0% for controls. (C) Change in fEPSP slopes relative to baseline stimulation in the LTP (red) or control (blue) hemispheres monitored for 2 hours prior to fixation. The average change in fEPSP slopes relative to baseline stimulation was 41% and 34% for the LTP (red) and 0% for control (blue) hemispheres. (D-G) Example electron micrographs and 3D reconstructions in the control and LTP hemispheres as indicated for each of the 4 animals. (Scale bars = 0.5 μm) Bottom row illustrates representative dendrites from control and LTP conditions in Animals 2 and 4 with segment lengths across the row of 9.25, 10.62, 9.44, and 11.33 μm, respectively. Axons synapsing on 15 spines along the middle of the dendrite were analyzed for presynaptic connectivity (solid yellow). Most of the axons (green) made synapses with just one dendritic spine, and some axons (white) made synapses with two dendritic spines (blue). Thus, the white axons illustrate the SDSA pairs. The dendritic shaft and spines occurring along the rest of the reconstructed dendrite are illustrated in translucent yellow. All excitatory synapses are illustrated in red, and the inhibitory synapses in purple. Scale cube = $1\mu m^3$.